SUPPLEMENTARY INFORMATION

Ion-driven nanograin formation in early-stage degradation of tri-cation perovskite films

Filipe Richheimer[‡,1,2], David Toth[‡,3,4], Bekele Hailegnaw[5,6], Mark A. Baker[2], Robert A. Dorey[2], Ferry Kienberger[3], Fernando A. Castro[1], Martin Kaltenbrunner[6], Markus C. Scharber[5], Georg Gramse[3,4] and Sebastian Wood[†,1]

1. National Physical Laboratory, Teddington, Middlesex, TW11 0LW, United Kingdom

2. Centre for Engineering Materials, University of Surrey, Guildford, GU2 7XH, United Kingdom

3. Keysight Technologies GmbH, Linz, 4020, Austria

4. Applied Experimental Biophysics, Johannes Kepler University, Linz, 4020, Austria

5. Linz Institute for Organic Solar Cells (LIOS), Johannes Kepler University, Linz, 4040, Austria

6. Department Soft Matter Physics (SoMaP), Johannes Kepler University Linz, 4040, Austria

‡ These authors contributed equally to this work

* Corresponding author: sebastian.wood@npl.co.uk

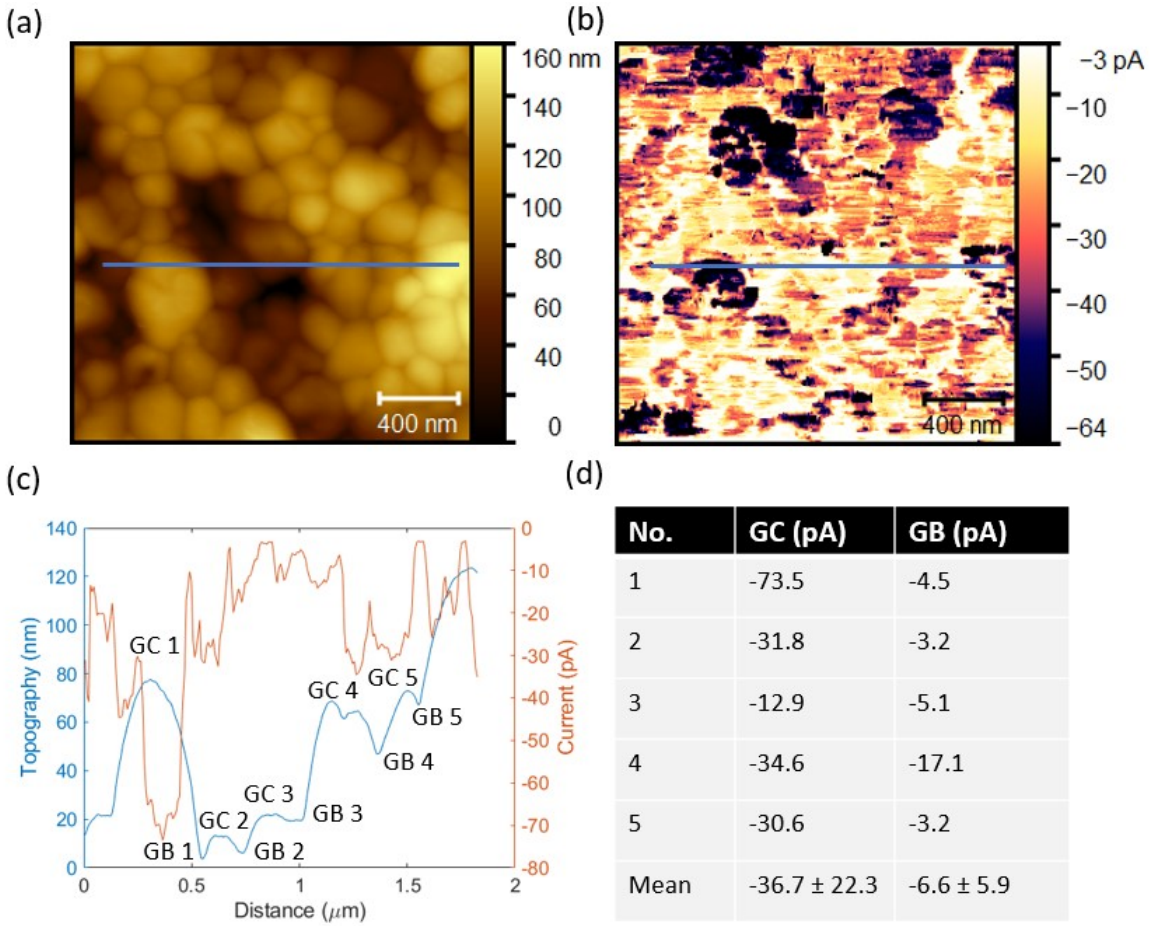

No.	GC (pA)	GB (pA)
1	-73.5	-4.5
2	-31.8	-3.2
3	-12.9	-5.1
4	-34.6	-17.1
5	-30.6	-3.2
Mean	-36.7 ± 22.3	-6.6 ± 5.9

Figure S1. Analysis of photocurrent differences between grain centres (GC) and grain boundaries (GB). (a) Topography and (b) pc-AFM scans with position of extracted cross-section in blue. (c) Combined plot of topography and current cross-sections with 5 GC and GB positions marked for current measurements. (d) Extracted GC and GB current values as marked in (c).

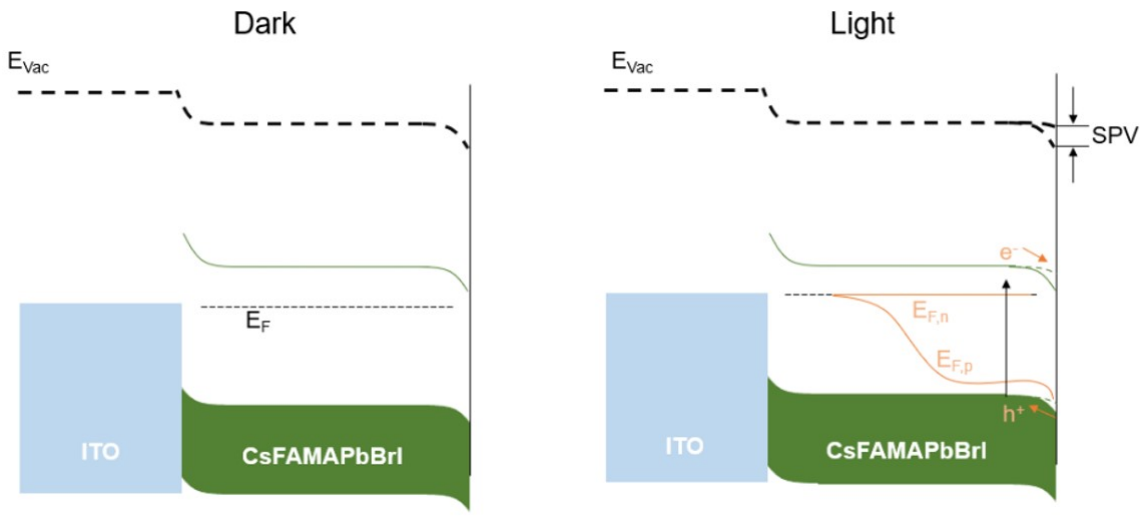

Figure S2. Band diagram of ITO/CsFAMAPbBrI/Free surface interface. Under dark conditions, Fermi levels of ITO and the OIHP layer are expected to lead to upwards band bending in a Schottky type contact. Surface states pin the Fermi level, resulting in a downward band bending at the free interface. When irradiated with light, electron and hole quasi-Fermi level splitting occurs in $E_{F,n}$ and $E_{F,p}$ respectively. Bands are flattened with electrons migrating towards the more p-type free surface with holes being repelled towards the film bulk. Overall SPV is given by the loss of band bending.

When the CsFAMAPbBrI is illuminated, the promotion of electrons from the valence band (VB) to the conduction band (CB) leads to quasi-Fermi level splitting into electron and hole Fermi levels respectively. In the volume close to the free surface, where the majority of incident photons is absorbed, photogenerated electrons and holes are spatially separated by band bending effects at the surface due to Fermi level pinning at surface states and dipoles. One electronic species will be attracted towards the surface by the space charge to counteract the resulting band bending, leading to a change in the surface potential and thus the measured CPD. The CPD difference between the sample under illumination and dark conditions is known as surface photovoltage (SPV) and defined as [1]

$$SPV \equiv CPD_{light} - CPD_{dark}.$$

Applying this relation, the SPV directly yields the direction of band bending.[1] Due to the positive SPV obtained in our measurements, downward band bending in towards the free surface is expected.

On the opposite interface between ITO and CsFAMAPbBrI the band alignment is inferred from values typically reported in literature. For ITO, work function values after plasma cleaning can reach close to 5.5 eV.[2] In a CsFAMAPbBrI composition, the work function at the surface was reported as approximately 4.6 eV when deposited on ITO.[3] It is important to use values obtained by measuring identical stacks of material, as the underlying layer can influence the Fermi level of the metal halide perovskite.[4] As a result, a Schottky type contact is expected, leading to an electron-depleted space charge at the OIHP back contact.

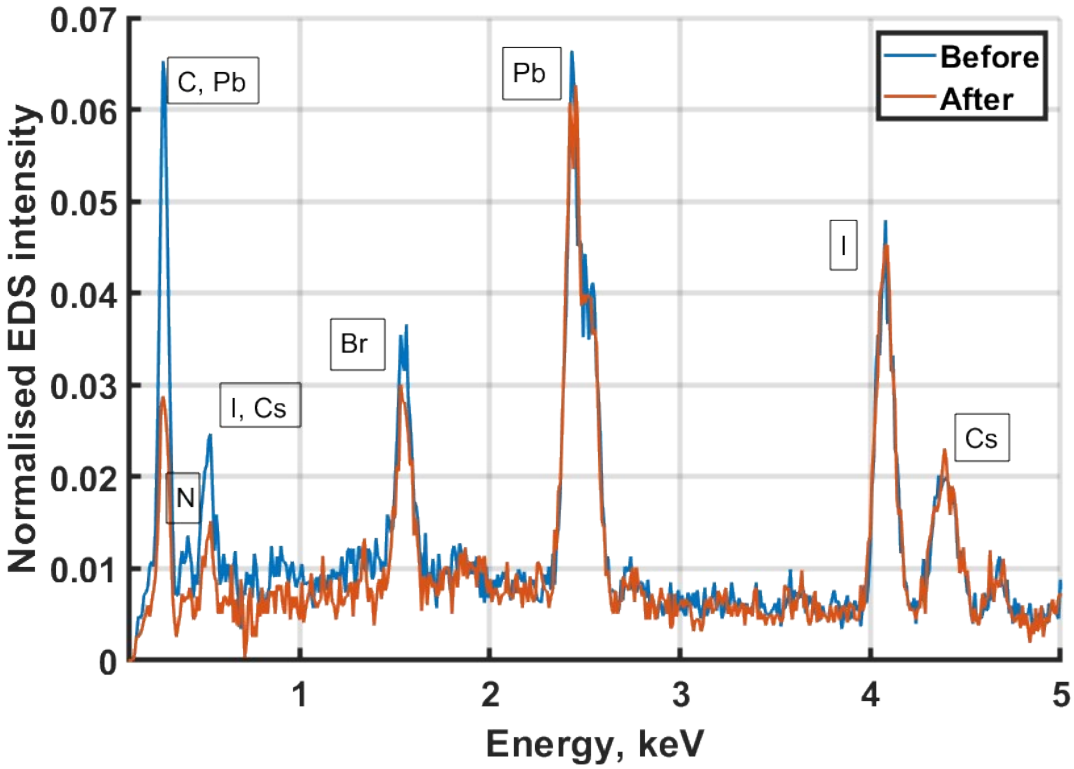

Figure S3. Energy dispersive X-ray spectra (EDX) of the perovskite film taken before and after illumination polling. 532 nm 10 sun (1000 mW/cm^2) illumination was used for 1 hour to induce degradation of the perovskite phase. As Pb content was not expected to suffer changes due to light induced degradation, spectra before and after illumination were normalized to the area of Pb peak found at ~2.5 keV.

Peaks weighted by Pb peak area in **Figure S2** were evaluated to assess elemental losses due to light induced degradation. Here, respective peak areas of (normalised) spectra before and after poling were integrated and ratios computed in the table below:

Peak ratio	C, Pb	N	I, Cs	Br	Pb	I	Cs
After/Before	0.50	0.59	0.58	0.82	1.00	1.04	1.03

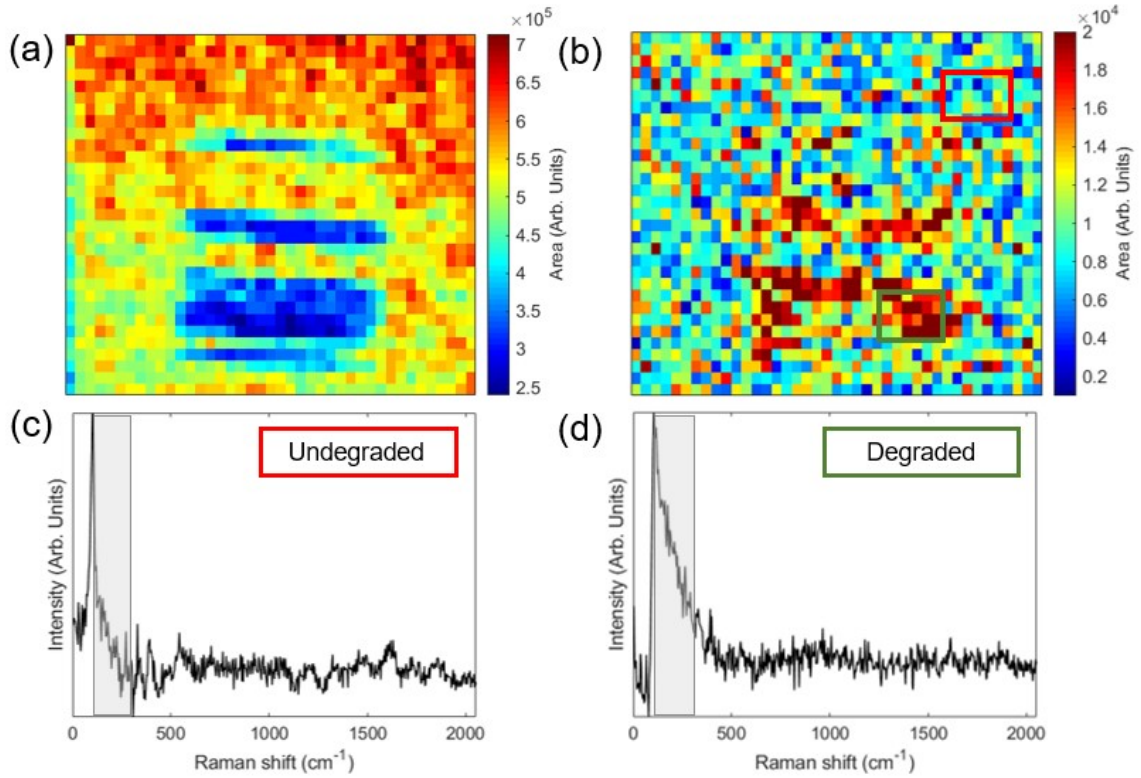

Figure S4. Raman spectroscopic mapping of area degraded with electrical poling using conductive AFM probe. Integrated intensity of 80-240 cm^{-1} Raman scattering (a) without and (b) with baseline correction. The integrated band is indicated by rectangular shaded area in (c) and (d). Averaged spectral areas of (c) undegraded and (d) degraded areas highlighted by blue and orange rectangles in (b).

Micro-Raman measurements were recorded inside the same LINKAM chamber used for thermal degradation experiments (later in Figure S8) under constant dry-N_2 gas flow. Raman spectra were recorded with a Horiba Labram confocal spectrometer and 532 nm laser excitation, using a long working distance objective (0.42 NA) to focus on the sample through the quartz window in the chamber. The results of the subsequent micro-Raman experiments are shown in Figure S4.

The degraded areas are formed of a set of separated horizontal stripes, with increasing widths from top to bottom and display an easily recognisable pattern. In Figure S4 (b) and (c), micro-Raman maps capturing the degraded and surrounding undegraded areas are shown. The integrated Raman bands from 80 cm^{-1} to 240 cm^{-1} are highlighted in Figure S4 (d) and (e) by the grey shaded areas. These incorporate the low wavenumber modes (<250 cm^{-1}) typically ascribed to lead halide products such as PbI_2 and $PbBr_2$.[5,6] The Raman maps in Figure S4 (b) and (c) correspond to the same integrated Raman bands, however in (c) we removed the background signal to highlight only changes due to the lead halide product peaks. Once the spectral background is removed using a high-order (10^{th} order) polynomial, (Figure S4 (c)) it is clear the degraded regions display higher counts at spectral ranges compatible with lead-halide decomposition.

The spectral changes of Raman spectra before and after electrical poling is shown by the averaged spectra of an undegraded and degraded area in Figure S4 (c) and (d). The spatially averaged spectra were extracted from inside the blue and orange rectangles outlined in Figure S4 (c) for undegraded and degraded spectra respectively. Both spectra were averaged against their highest intensity feature to highlight relative changes. Here, is it apparent that a large increase in counts close to the cut-off of the Raman edge filter at ~100 cm^{-1} is present after degradation. These experiments further confirm that the early stage degradation products in the form of nanograins are composed of lead halide resulting from a decomposition of the perovskite phase.

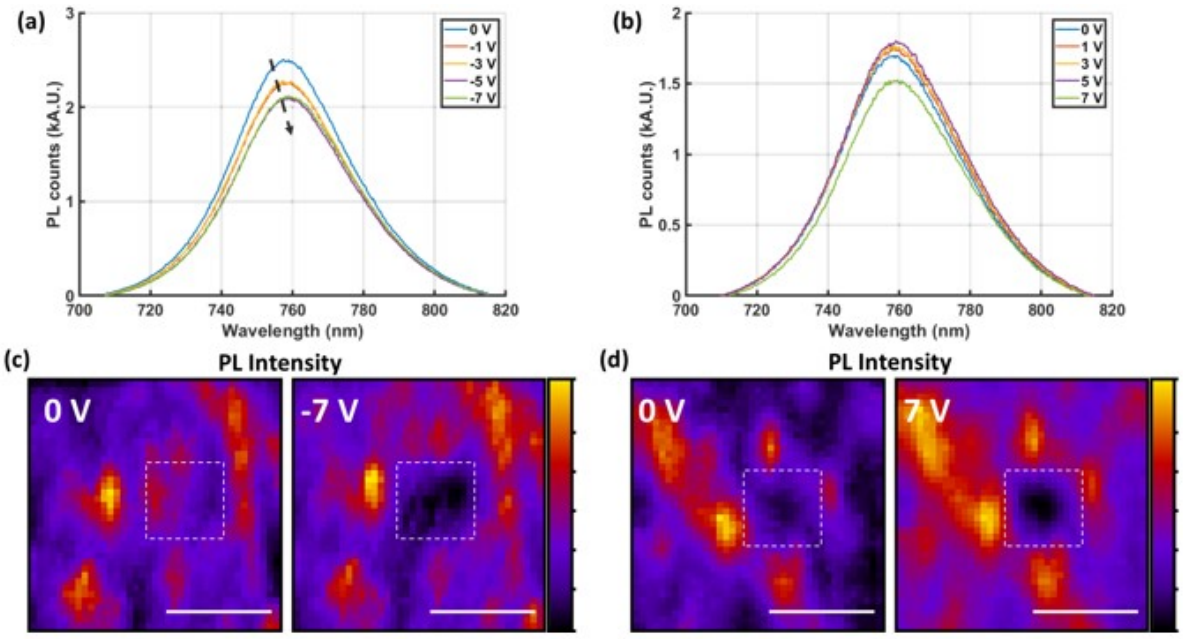

Figure S5. Photoluminescence imaging of short-circuit poled area inside white square. (a) PL spectra taken after localized short-circuit polling with various negative biases applied to the AFM tip. (b) PL spectra taken after localized short-circuit polling with various positive biases applied to the AFM tip. (c) Map of PL peak intensity before and after -7 V short-circuit polling. (d) Map of PL peak intensity before and after 7 V short-circuit polling. Scale bar is 8 µm.

For increasing magnitudes of negative bias a continuous decrease in PL peak intensity is observed. In contrast, increasing magnitudes of positive bias poling result in an initial increase in PL peak intensity, followed by a sharp decrease at 7 V. Loss in PL intensity is primarily related to a decrease in radiative recombination of photoinduced charges. Previous work reported laser-induced perovskite decomposition into PbI_2 to have a detrimental effect on PL signal when present in sufficiently high amounts to be detected by chemically selective techniques.[7] Initial PL peak intensity increases for positive poling indicate improved radiative recombination. The formation of a thin (<20 nm) lead-halide shell at grain surfaces has been suggested to passivate trap sites acting as non-radiative recombination centers.[7] Alternatively, the poling induced charge redistribution may itself lead to local neutralization of these non-radiative recombination centers.[8] Such an effect would act similarly to pre-conditioning, where initial exposure to light or electric field improves operational conditions of perovskite solar cells.

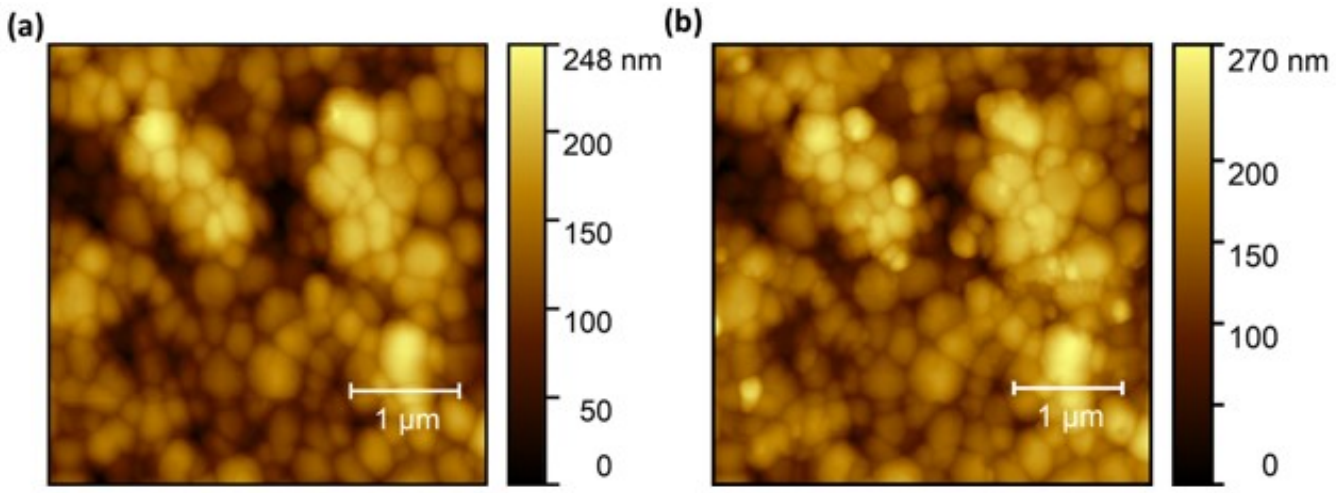

Figure S6. Light induced nanograins. (a) Topography image taken before illumination. (b) Topography image taken after an illumination period of 88 hours with a 532 nm monochromatic beam at an intensity of ~ 1 sun.

Lower illumination intensity was used to demonstrate relevance of growth of NGs under conditions relevant to solar cell operation. Here the sample surface was illuminated with a 532 nm wavelength monochromatic beam at an intensity of ~ 1 sun (80 mW/cm^2), in contrast to the 633 nm wavelength beam and 3.36 kW/cm^2 intensity utilized in the main text. The formation of NG features under across such a wide range of conditions may be partially explained by wavelength dependence of the absorption spectrum, leading to differences in resulting photogenerated charge densities. Such dependence has been previously observed for ionic and trap site migration in perovskites.[7,8]

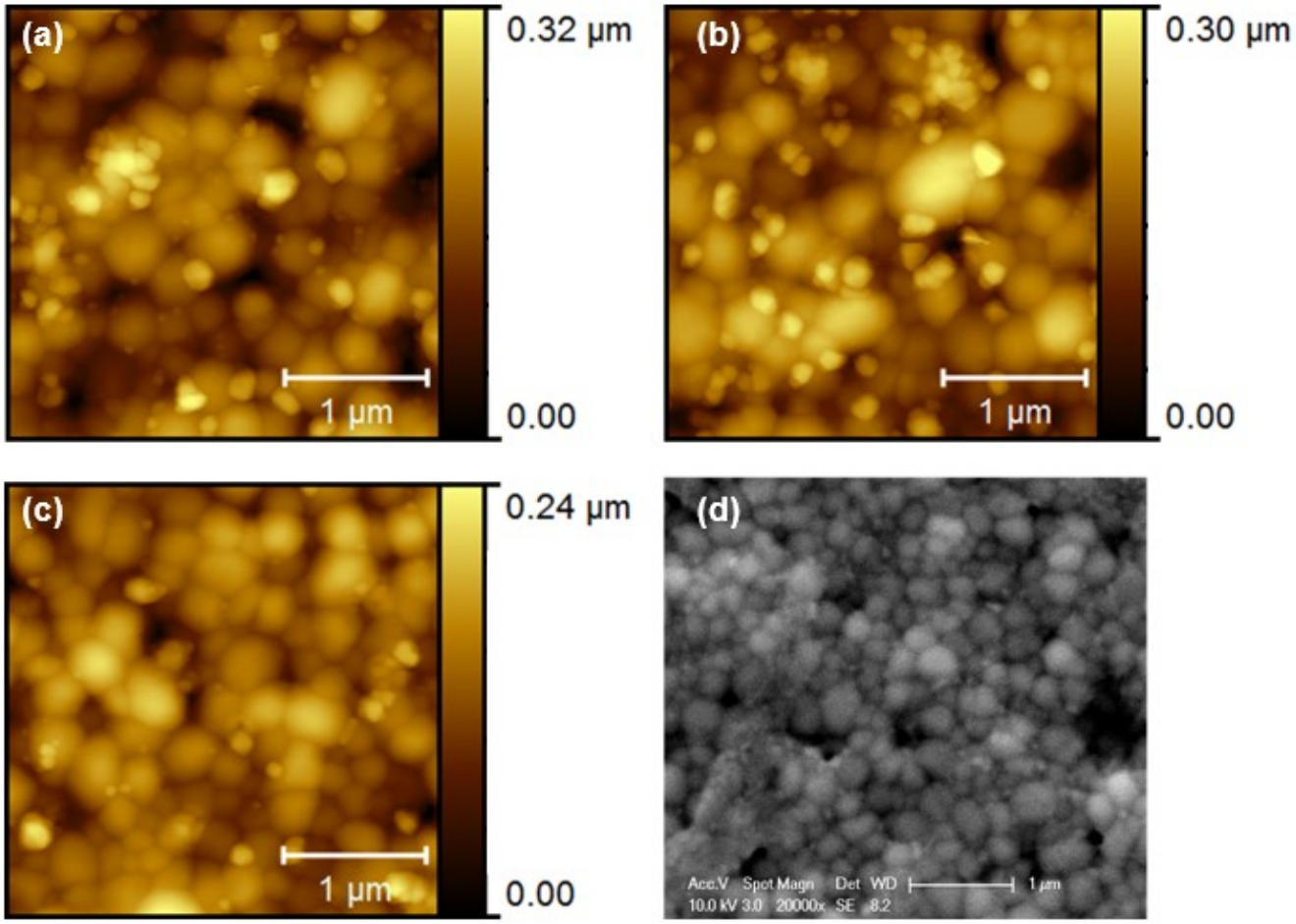

Figure S7. Perovskite films degraded in ambient conditions. (a-c) Tapping AFM topography images taken of a CsFAMAPbBrI film after degradation in ambient conditions. (b) Repeated from main text. (d) SEM image taken on ambient degraded CsFAMAPbBrI film.

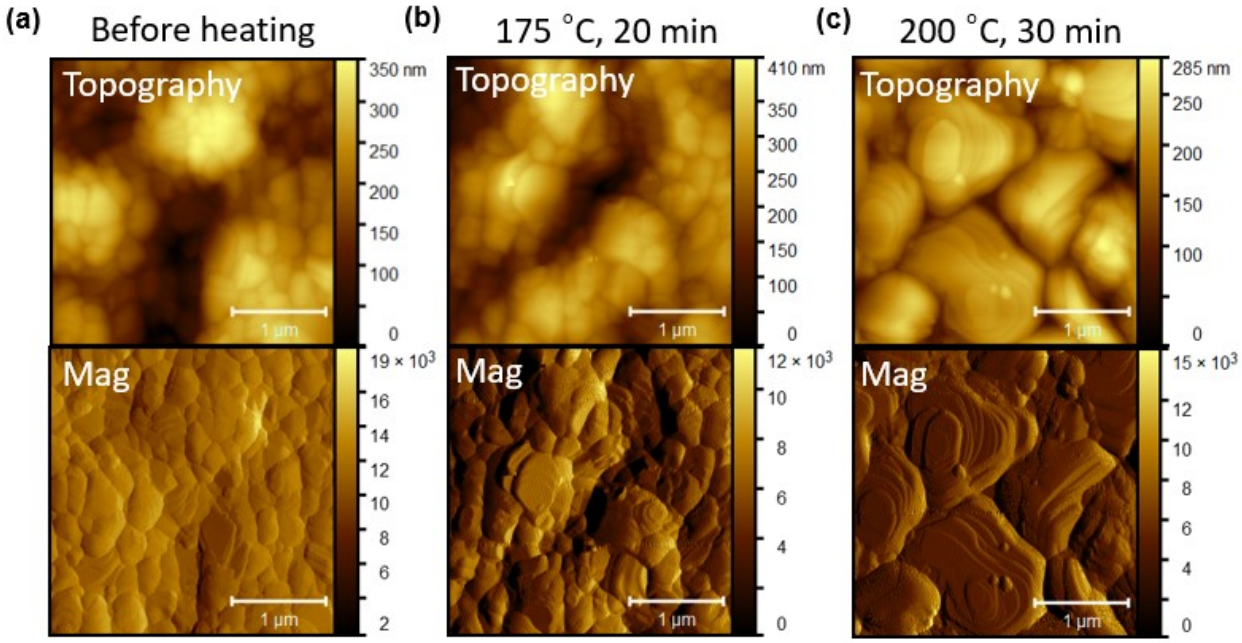

Figure S8. Alternating measurements of surface topography and exposure to hotplate at increasing temperatures under inert atmosphere. (a) Initial AFM topography and amplitude modulation error signal (Mag) of pristine CsFAMAPbBrI film surface. (b) Topography and Mag signal after 20 min hotplate at 175 °C under constant N_2 flow. (c) Topography and Mag signal after subsequent 30 min hotplate at 200 °C under constant N_2 flow.

Topography and hotplate measurements were performed by measuring topography in glovebox-enclosed AFM system and subsequently heating the sample in a LINKAM chamber under dry-nitrogen flow. Between each heating stage temperature was incremented by 25 °C, starting at 100 °C and terminating at 200 °C. Temperature was ramped at 15 °C/min and once desired temperature reached the sample was left for 20 to 30 min. Sample loading and offloading to sealed chamber was performed inside glovebox, preventing sample exposure to ambient during experimental cycle. Surface structure was largely unchanged until heating at 175 °C. Additional heating effects such as local thermal gradients which can impact the crystal formation are not captured by this study and require a more detailed investigation.

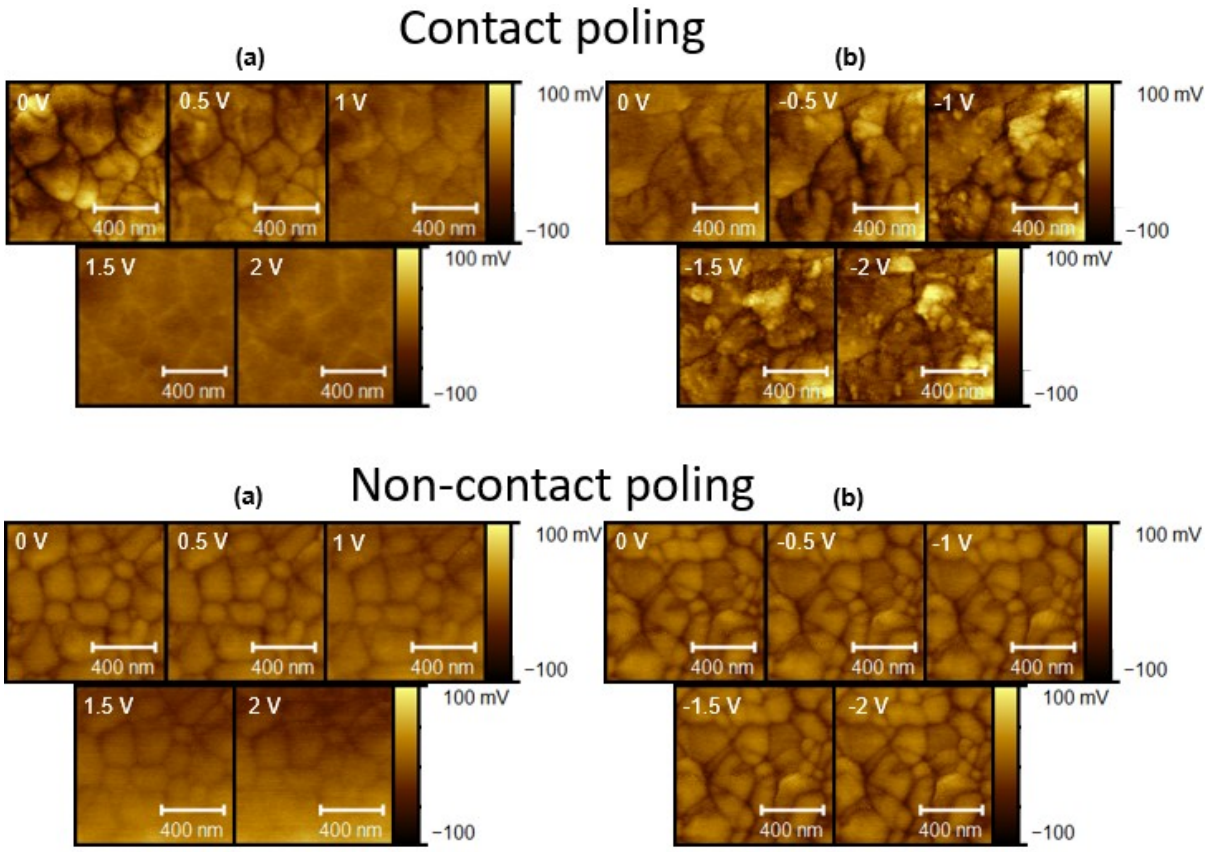

Figure S9. Complete set of post-poling KPFM maps. V_{CPD} average of each map was subtracted to highlight local contrast in the polycrystalline structure. Previous poling was performed with probe in contact with sample applying (a) positive and (b) negative bias to the probe and in non-contact applying (c) positive and (d) negative bias to the probe.

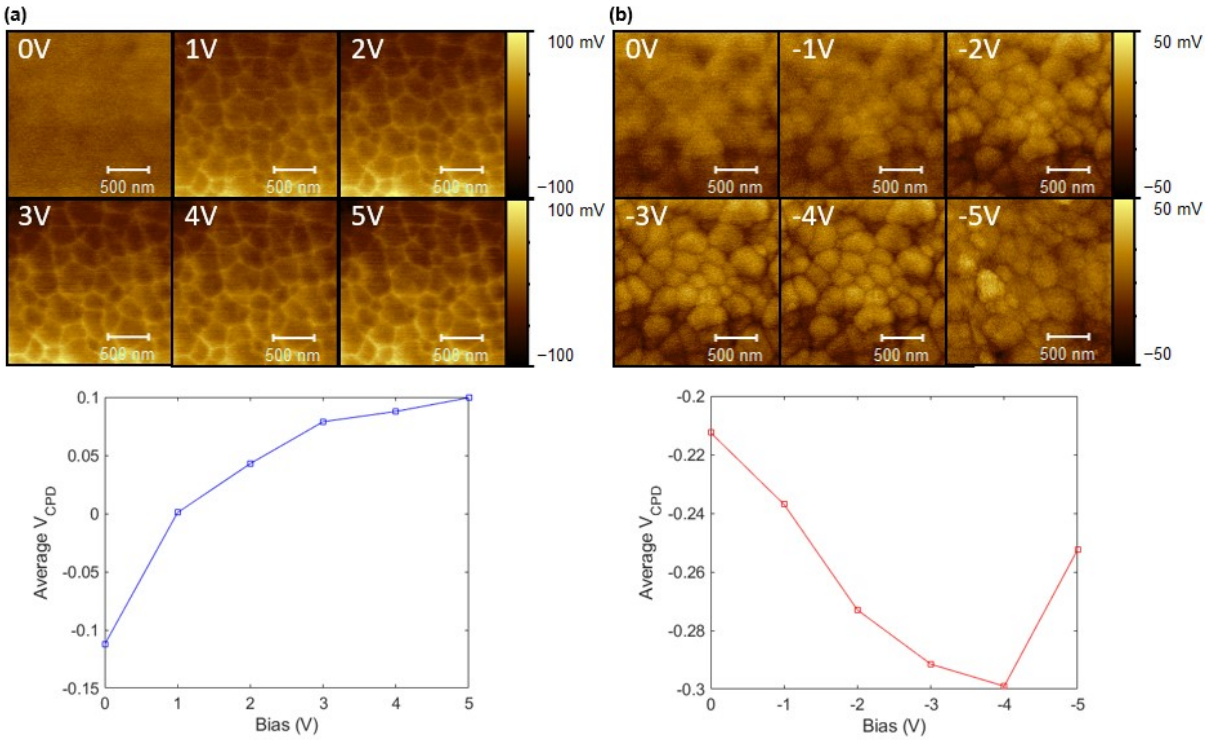

Figure S10. Extended voltage range in non-contact poling. Each subfigure shows spatially resolved KPFM maps after subtracting V_{CPD} average, which is plotted in the respective line plot below. Non-contact poling performed under (a) positive and (b) negative bias applied to the probe.

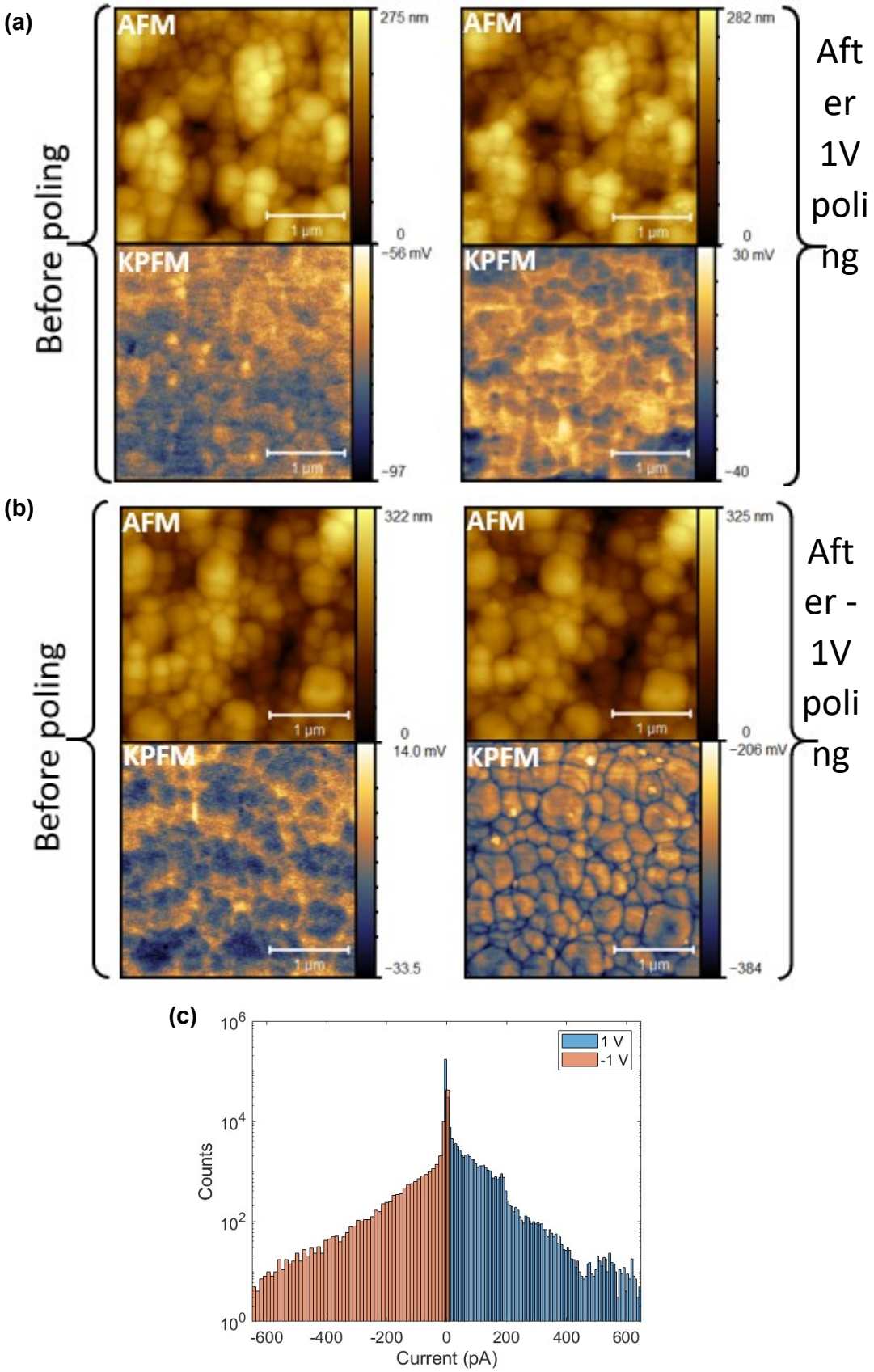

Figure S11. Comparison of topography (AFM) and surface potential (KPFM) data before and after polling with simultaneous electrical and optical stressors. Polling experiment with (a) 1 V and (b) -1 V applied to the AFM probe under illumination of approximately 1 sun (100 mW/cm^2), of 532 nm monochromatic radiation. (c) Histogram representation of positive and negative bias poling PC-AFM.

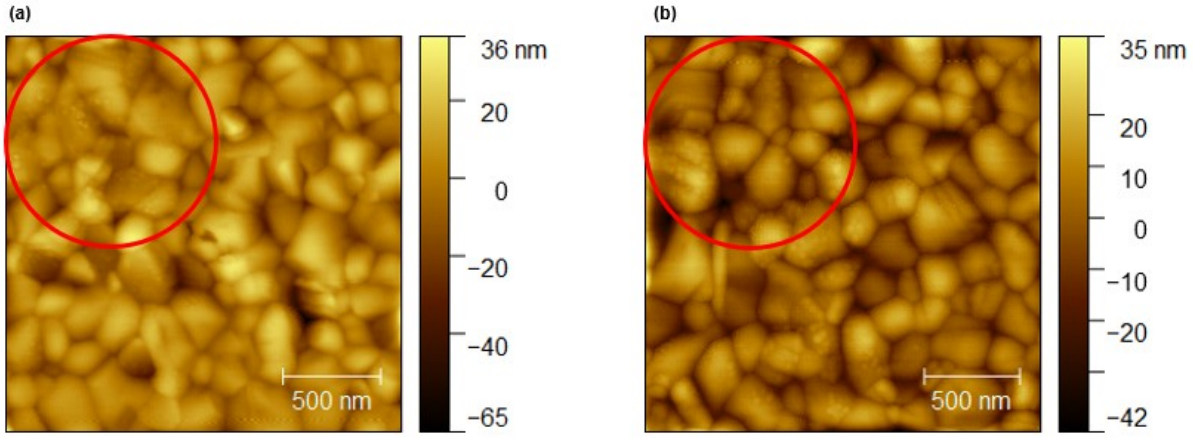

Figure S12. Effect of applied static electric field to nanograin formation. (a) Topography of the perovskite after polling with 633 nm ~1.05 kW/cm^2 illumination and -9 V applied to the sample. (b) Topography of the perovskite after polling with 633 nm ~1.05 kW/cm^2 illumination and +9 V applied to the sample. The same illumination without applied bias did not result in formation of nanograins.

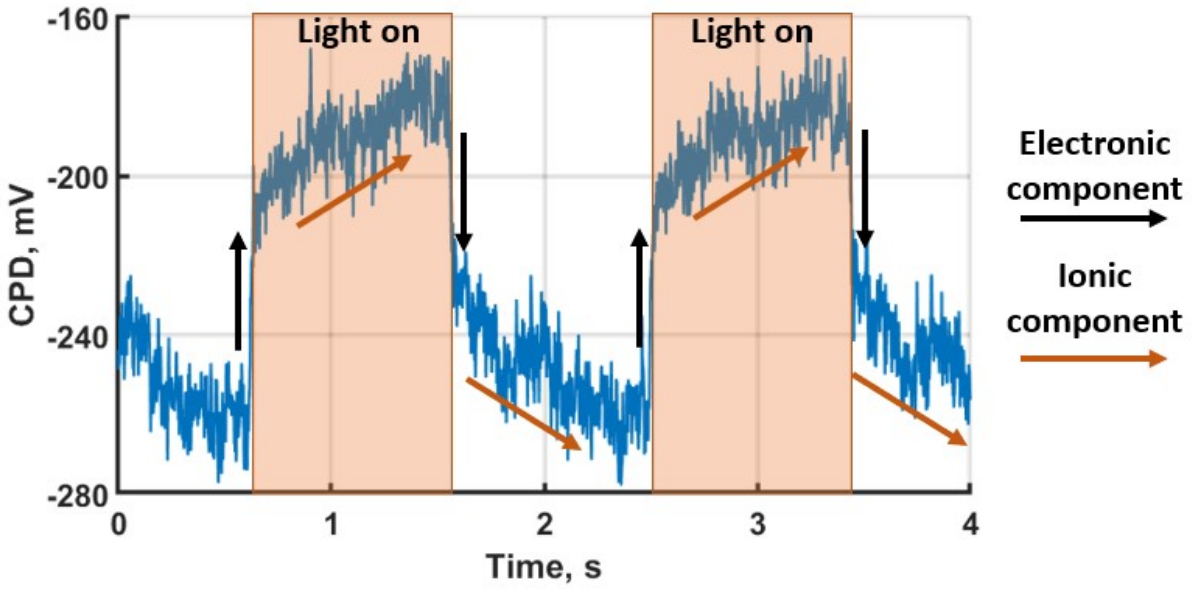

Figure S13: KPFM measurement time series for two subsequent light pulses. Sharp transitions with changes in illumination conditions reflect electronic components of charge redistribution, whilst slow transients relate to ionic contributions.

References

1 S. Sadewasser and T. Glatzel, *Kelvin Probe Force Microscopy: From Single Charge Detection to Device Characterization*, Springer, 2018.

2 I. Irfan, S. Graber, F. So, Y. Gao, *Org. Electron.*, 2012, **13**, 2028.

3 X. Zheng, Y. Hou, C. Bao, J. Yin, F. Yuan, Z. Huang, K. Song, J. Liu, J. Troughton, N. Gasparini, C. Zhou, Y. Lin, D.J. Xue, B. Chen, A.K. Johnston, N. Wei, M.N. Hedhili, M. Wei, A.Y. Alsalloum, P. Maity, B. Turedi, C. Yang, D. Baran, T.D. Anthopoulos, Y. Han, Z.H. Lu, O.F. Mohammed, F. Gao, E.H. Sargent, O.M. Bakr, *Nat. Energy,* 2020, **5**, 131–140.

4 M. Daboczi, I. Hamilton, S. Xu, J. Luke, S. Limbu, J. Lee, M.A. McLachlan, K. Lee, J.R. Durrant, I.D. Baikie, J.S. Kim, *ACS Appl. Mater. Interfaces.*, 2019, **11**, 46808–46817.

5 P. Pistor, A. Ruiz, A. Cabot and V. Izquierdo-Roca, *Sci. Rep.*, 2016, **6**, 1–8.

6 S. Ruan, D. P. McMeekin, R. Fan, N. A. S. Webster, H. Ebendorff-Heidepriem, Y. B. Cheng, J. Lu, Y. Ruan and C. R. McNeill, *J. Phys. Chem. C*, 2020, **124**, 2265–2272.

7 J. Barbé, M. Newman, S. Lilliu, V. Kumar, H.K.H. Lee, C. Charbonneau, C. Rodenburg, D. Lidzey, W.C. Tsoi, *J. Mater. Chem. A*, 2018, **6**, 23010–23018.

8 D.W. DeQuilettes, W. Zhang, V.M. Burlakov, D.J. Graham, T. Leijtens, A. Osherov, V. Bulović, H.J. Snaith, D.S. Ginger, S.D. Stranks, *Nat. Commun.*, 2016, **7**, 11683.